DE GRUYTER Z. Kristallogr. 2018; 233(1): 9–16

Arjun Kalra, Mingtao Zhang, Sean Parkin and Tonglei Li*

Crystal packing and crystallization tendency from the melt of 2-((2-ethylphenyl)amino)nicotinic acid

https://doi.org/10.1515/zkri-2017-2070
Received April 23, 2017; accepted August 5, 2017; published online September 19, 2017

Abstract: 2-((2-ethylphenyl)amino)nicotinic acid (2EPNA) was synthesized and its crystal structure was determined. It was observed that alkylation of the phenyl ring with ethyl group disrupts the planar conformation of the molecule by steric repulsion, resulting in formation of an acid-pyridine heterosynthon (instead of acid-acid homosynthon) in the crystal. Crystallization tendency from the melt state of the polymorph was studied by differential scanning calorimetry (DSC). It was revealed that this compound could form a very stable amorphous phase on melt quenching and not crystallize even on re-heating. The formation of acid-pyridine hydrogen bonding in the amorphous state is believed to be responsible for its good glass forming ability.

Keywords: amorphous; crystal structure; DSC; NMR; polymorphism.

Introduction

Understanding the structure-property relationship of organic compounds is critical for controlling the bulk properties of materials [1–4]. Considerable research efforts have been devoted towards predicting the crystal packing of compounds based on their molecular structures [5–7]. The impact of molecular structure on formation of amorphous solids has emerged as an active field. Better understanding of glass formation and stability permits the use of amorphous materials for a wide range of applications ranging from food [8] to opto-electronics [1] and to pharmaceutical products [9]. In drug development, amorphous drug products are used for enhancing the solubility of poorly water-soluble drug molecules. However, this metastable state has a tendency to crystallize, which impacts the safety and efficacy of the products [10–12].

Previous work in our laboratory examined the relationship between intermolecular interactions and conformation through crystal engineering. By covalently linking bulky alkyl or electron-withdrawing groups to the phenyl ring of diarylamine compounds, we investigated how the molecular structure influences the hydrogen bonding motif in the crystal [13–16]. It was observed that bulky alkyl groups lead to crystal structures with the acid-pyridine synthon because of the groups' ability to destabilize the planar conformation by steric repulsion and expose the pyridine nitrogen [15]. On the other hand, linking an electron-withdrawing group leads to the acid-acid synthon in the crystals because of the ability of the functional group to reinforce the π-conjugation in the molecule, and therefore strengthen the planar conformation [14].

We have recently utilized a series of structurally similar diarylamine compounds to study the structure-amorphization relationship. By introducing various structural elements to the same diarylamine scaffold, we studied the role of molecular structure on glass formation and stability. We found that in this family of compounds, hydrogen bonding between carboxylic acid and pyridine nitrogen contributes to glass formation by generating supramolecular aggregates that hinder crystallization [17]. One of the compounds we studied was 2-((2-ethylphenyl)amino)nicotinic acid (2EPNA) (Scheme 1a). Herein, we report the synthesis, polymorph screening, and crystal structure of the compound. The glass forming ability of this compound was evaluated using thermal analysis; the solid forms were characterized by spectroscopic analysis. It is concluded that, because of the presence of a large bulky group on the phenyl ring, this compound crystallizes with an acid-pyridine synthon that contributes to its good glass forming ability.

Experimental

Materials

2-Chloronicotinic acid (98% purity), aniline (ACS grade), pyridine (ACS grade), and *p*-toluenesulfonic acid (98% purity) were purchased

---

***Corresponding author: Tonglei Li,** PhD, Department of Industrial and Physical Pharmacy, College of Pharmacy, Purdue University, RHPH Building, Room 124B, 575 Stadium Mall Drive, West Lafayette, IN 47907-2091, USA, Tel.: (765) 494-1451,
E-mail: tonglei@purdue.edu
Arjun Kalra and Mingtao Zhang: Department of Industrial and Physical Pharmacy, College of Pharmacy, Purdue University, West Lafayette, IN 47907, USA
Sean Parkin: Department of Chemistry, University of Kentucky, Lexington, KY 40536, USA

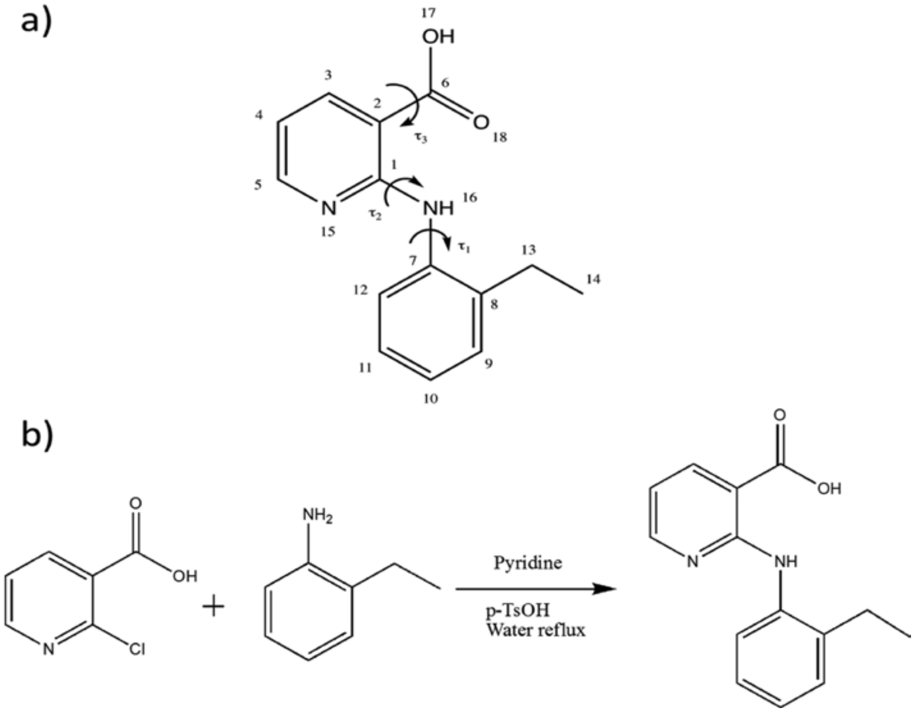

Scheme 1: Chemical structure of 2EPNA (a) and synthetic scheme for 2EPNA (b). Torsion angles (τ) are marked. The atomic numbering for non-hydrogen atoms is also marked.

from Sigma-Aldrich (St. Louis, MO, USA). Methanol, hexane, toluene, acetone, ethyl acetate, chloroform, and dichloromethane were purchased from Macron (Center Valley, PA, USA). Ethanol (200 proof) was obtained from Decon Labs (King of Prussia, PA, USA). Deuterated dimethyl sulfoxide (DMSO-d6) was purchased from Cambridge Isotope Inc. (Tewksbury, MA, USA).

Synthesis and characterization

2-Chloronicotinic acid (4 g, 25.3 mmol), aniline (3.07 g, 25.3 mmol), pyridine (2.0 g, 25.3 mmol), and *p*-toluenesulfonic acid (1.0 g, 6.0 mmol) were added to a round-bottom flask, followed by addition of 40 mL of water. The resulting mixture was refluxed overnight. The reaction mixture was cooled to room temperature and the resulting crystals were retrieved by filtration [15]. The synthetic scheme is shown in Scheme 1b. Solution NMR spectroscopy (Bruker ARX500; BBO probe) was used to verify the chemical structures of the synthesized compound.

^{1}H NMR (DMSO-*d6*, 500 MHz): δ 13.5 (s, 1H), 10.3 (s, 1H), 8.3 (dd, 1H), 8.2 (dd, 1H), 8.1 (d, 1H), 7.2 (d, 1H), 7.1 (t, 1H), 7.0 (t, 1H), 6.8 (dd, 1H), 2.6 (q, 2H), 1.1 (t, 3H).

FTIR (cm^{-1}): 3264, 3065, 3027, 2968, 2930, 2871, 1658, 1594, 1580, 1504, 1396, 1250, 1225, 1189, 1142, 816, 756.

Crystal structure determination

The crystals cracked when cooled to 90 K, but were stable and remained intact above 180 K. X-ray diffraction data were collected at 200(2) K on a Bruker-Nonius X8 Proteum diffractometer with graded-multilayer focused CuK(α) X-rays. Raw data were integrated, scaled, merged and corrected for Lorentz-polarization effects using the APEX2 package [18]. Corrections for absorption were applied using SADABS [19]. The structure was solved by direct methods (SHELXT) [20] and refined against F^2 by weighted full-matrix least-squares (SHELXL-2014) [21]. Hydrogen atoms were found in difference maps but subsequently placed at calculated positions and refined using a riding model. Non-hydrogen atoms were refined with anisotropic displacement parameters. The final structure model was checked using an R-tensor [22] and by Platon/checkCIF [23]. Atomic scattering factors were taken from the International Tables for Crystallography [24].

X-ray powder diffraction (XRPD)

A Rigaku Smartlab (The Woodlands, TX, USA) diffractometer (in the Bragg-Brentano configuration) with Cu Kα radiation (40 kV, 40 mA) was used for collecting powder diffraction data. Diffraction patterns were collected between 4.0° and 40.0° 2θ with a step size of 0.02° and scan rate of 4°/min.

Differential scanning calorimeter

A DSC Q2000 (TA instruments, New Castle, DE, USA) equipped with a refrigerated cooling system (RCS 90) and an auto-sampler was used for thermal analysis. Samples were placed in a hermetically sealed Tzero pan/lid system and heated at 10 °C/min to 418.1 K. After waiting for 3 min, the melt was cooled at 20 °C/min. Finally, the sample was re-heated at 10 °C/min to 418.1 K.

Crystal growth and optical microscopy

The compound recovered from the reaction mixture was colorless. The solid was then dissolved in a variety of solvents and the solutions were allowed to evaporate until crystals formed. An Olympus SXZ12 microscope (Shinjuku, Japan) was used to image the crystalline samples.

Solid-state NMR spectroscopy

A Chemagnetic CMX 400 MHz ($^1H = 399.82$ MHz; $^{13}C = 100.55$ MHz) spectrometer was used to obtain the spectra of crystalline and amorphous samples of 2EPNA. Samples were packed in a 5 mm zirconia rotor and ^{13}C spectra were obtained with cross-polarization/magic-angle spinning (CP/MAS) and total sideband suppression (TOSS) at ambient temperature. Operating conditions included a spinning speed of 6 kHz, acquisition time of 16 ms, TPPM high-power proton decoupling, and a ^1H pulse width of 5 µs (90°). A CP contact time of 3.5 ms was used for all samples. A delay time of 50 s was employed for the crystalline sample, while a shorter delay time of 10 s was used for the amorphous sample.

NMR chemical shift calculations and conformational analysis

NMR chemical shielding was calculated using the gauge-invariant atomic orbital (GIAO) method [25–28]. Atomic coordinates for a single molecule were extracted from the crystal structure and a full optimization was done under the level of B3LYP/6-311++g(d,p). Then NMR calculations were run under the level of B3PW91/6-311g++(d,p). NMR calculations were run for a partially optimized (all non-hydrogen atoms were fixed) single molecule and for a dimer extracted from crystal structure. Calculated isotropic chemical shielding was converted to a chemical shift value by: $\delta_{iso} = \sigma_{ref} - \sigma_{calc}$, where the isotropic chemical shift (δ_{iso}) was obtained as the difference between the chemical shielding of a reference molecule – tetra methyl silane (TMS) – (σ_{ref}) and the calculated shielding value (σ_{calc}) [29].

The conformational energy of the 2EPNA single molecule was evaluated with Gaussian 09/C.01 [30] (Gaussian, Inc., Wallingford, CT, USA) under the level of HF/6-311++G(d,p). Each torsion angle was scanned with all bond lengths, bond angles, and other torsion angles allowed full flexibility to find the energy minima.

The crystal structure of 2EPNA was optimized by Crystal14 [31] at the level of PW1PW/6-21G(d,p) with the lattice parameters kept constant. The optimized crystal structure was further evaluated for calculating electron densities and Hirshfeld surface. Fukui functions and electrostatic potential (ESP) calculated from the optimized single molecule were respectively mapped onto the Hirshfeld surface. The results were analyzed and processed by a program developed in our laboratory, which also generated input files used by OpenDX for visualization [32].

Results and discussion

Crystal packing

Polymorph screening was performed in a variety of solvents (ethanol, methanol, acetonitrile, methanol, hexane, toluene, acetone, ethyl acetate, chloroform, dichloromethane, water). The crystals collected from all experiments showed similar colorless blocks (Figure 1). Subsequently, the structure of the crystallized form (called Form I) was determined. The crystallographic data are presented in Table 1. For the complete CIF file, see Supporting Information (CCDC deposition number is 1543341).

Form I is monoclinic with space group of $P2_1/n$ (Figure 2a). The asymmetric unit consists of one crystallographically independent molecule. The molecules form one-dimensional supramolecular chains through intermolecular O–H···N hydrogen bonds between the OH of the carboxyl and N of the pyridine ring (C(6) by the graph set concept [33]) (Figure 2b). The chains further stack upon each other along the b axis. The distance between O and N is 2.666 Å with the angle between O–H···N being 172.14°. The intramolecular hydrogen bond between the amine and carbonyl O can be identified with the distance between N and O as 2.680 Å and angle between N–H···O being 138.17°. Figure 3 shows the comparison between the experimental XRPD and the powder pattern simulated

Fig. 1: 2EPNA crystals observed under the microscope. The large clump is about 1 mm × 0.5 mm, and the individual single crystals are plates, about 0.1–0.2 mm across.

Tab. 1: Crystallographic data of 2EPNA.

	Form I
Morphology	Colorless blocks
Space group	$P2_1/n$
a/Å	8.9247 (2)
b/Å	14.0340 (2)
c/Å	10.9795 (2)
α/deg	90.0
β/deg	107.139 (1)
γ/deg	90.0
Z′	1
Z	4
$V/Å^3$	1278.20
$D_{cal}/g \cdot cm^{-3}$	1.259
R_1	0.0373
T/K	200
R (int)	0.0505
S	1.033
θ range for data collection	5.359–68.407°
Data/restraints/parameters	2333/0/170
Limiting indices	$-10 \le h \le 10$, $-7 \le k \le 16$, $-12 \le l \le 12$

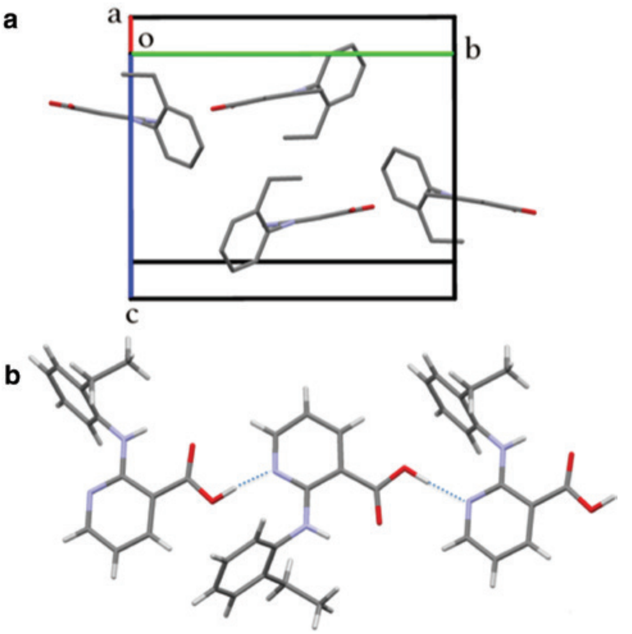

Fig. 2: Crystal packing of 2EPNA. (a) unit cell (b) hydrogen bonding synthon in 2EPNA.

from the single-crystal structure, demonstrating the phase purity.

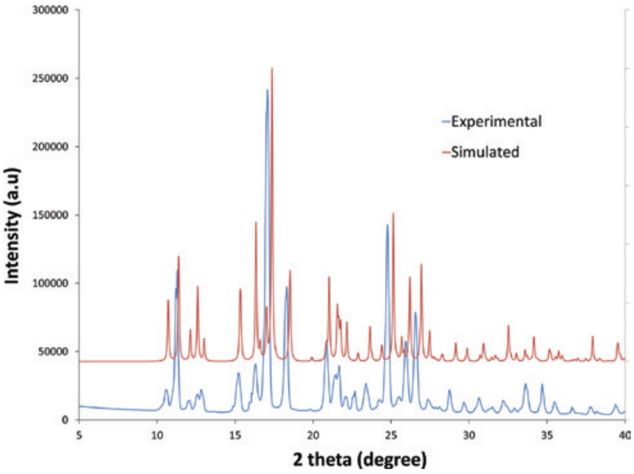

Fig. 3: Experimental and simulated powder X-ray diffraction patterns of 2EPNA (λ = 1.54056 Å).

Two important packing motifs – formation of acid-pyridine hydrogen bonding chains and π–π stacking between molecules in adjacent chains – can be identified in the crystal structure of 2EPNA. These packing features were rationalized by mapping the electrostatic potential (ESP) and Fukui functions on its Hirshfeld surface. The molecular ESP of 2EPNA is shown in Figure 4a and highlights the local hardness [34]. The positive and negative regions of ESP can be observed at the –OH and pyridine nitrogen, respectively. These groups are associated with the hydrogen bonding in the crystal structure. It is known that hydrogen bonding bears an electrostatic interaction

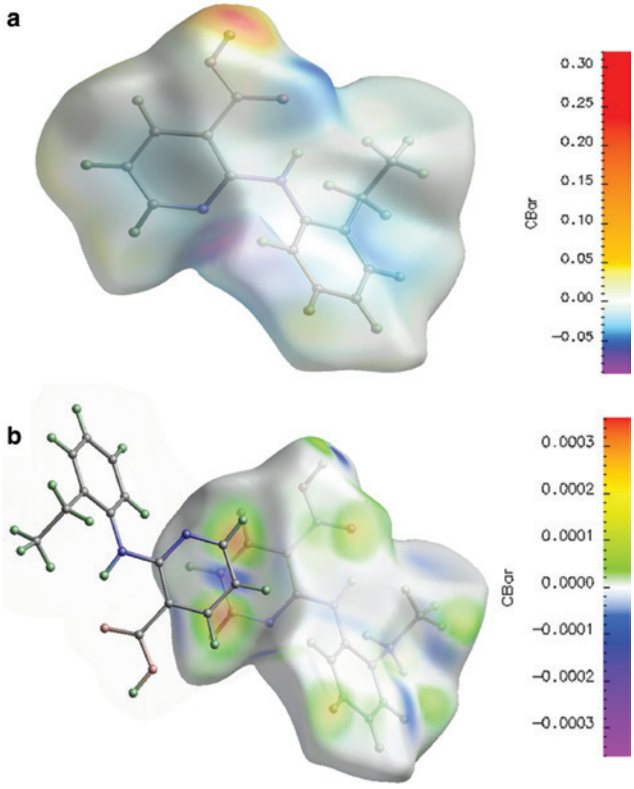

Fig. 4: Hirshfeld surfaces of 2EPNA showing mapped molecular electrostatic potential (ESP) (a) and Fukui function (b). The units for ESP and Fukui function are hartrees and electron/bohr³, respectively.

component, and thus local hardness is associated with this type of interaction. In addition, the Fukui function characterizes local softness [34]. Fukui functions can be seen at the hydrogen-bonding region as these interactions also contain soft-soft components. Figure 4b shows the Fukui function (f^2, dual descriptor [35]) mapped on the Hirshfeld surface for two molecules involved in π–π stacking. A soft region of a molecule, indicated by large positive or negative f^2 values, prefers interacting with a soft region of another molecule [34]. The π–π stacking between these molecules follows this principle with the Fukui function hotspots showing the region of maximum interaction.

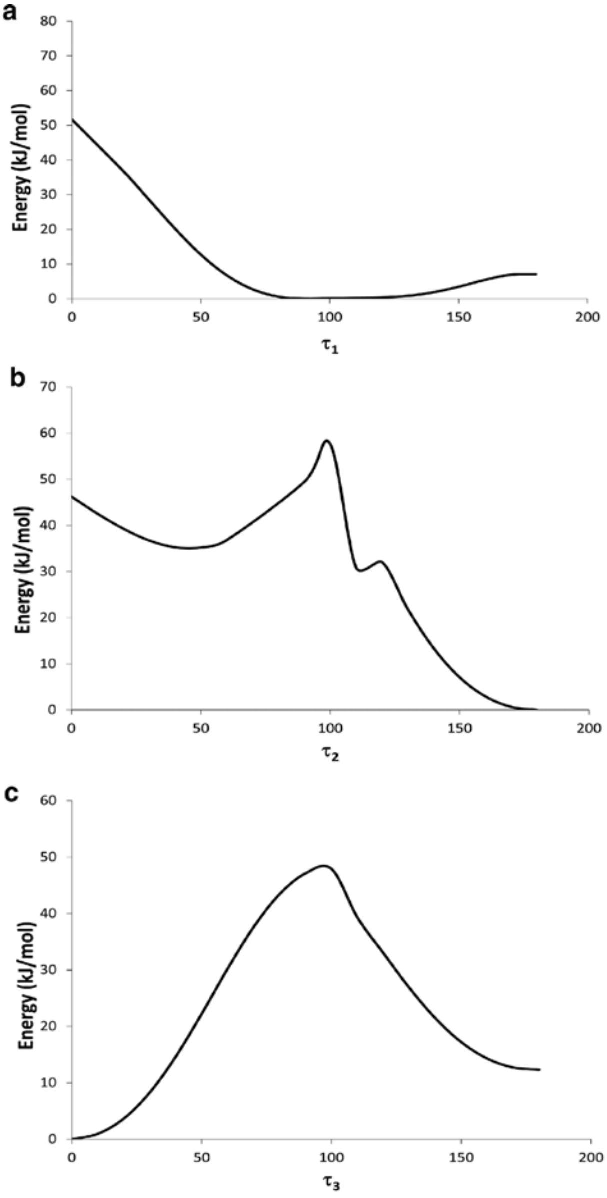

Fig. 5: Conformational energy scan of τ_1 (a), τ_2 (b) and τ_3 (c) of single 2EPNA molecule.

The molecule has three conformational degrees of freedom, designated as τ_1, τ_2 and τ_3 (Scheme 1a). Conformational energy versus torsion angle is plotted in Figure 5. The global minimum for τ_1 is at 90° (Figure 5a). Within 80°–130° torsion angles there is a very small energy difference (around 2 kJ/mol) between the conformers (Figure 5a). For the crystallized polymorph, this dihedral angle is observed at 123.62°, within this energy minima. The difference from the calculated energy-minimal angle is likely due to contributions by intermolecular interactions in the crystal. The global minimum for τ_2 coincides with the planar conformation (Figure 5b). The torsion angle in the crystal structure is close to this global minimum, with a value of 168.71°. The dihedral angle τ_3 in the crystal structure was observed at –0.42° with the –COOH functional group adopting the *syn* conformation with the carbonyl O forming an intramolecular hydrogen bond with N–H of the diarylamine, leading to an S(6) motif. Based on the conformational energy scan of this torsion angle (Figure 5c), the energy minima is located at 0°, which is in accordance with the experimental value. These results show that all three dihedral angles are close to their global minimum values, suggesting that this crystalline form might be the most stable polymorph for this molecule.

Crystallization from melt

Thermal properties of the compound were studied using differential scanning calorimetry (DSC) (Figure 6). The melting onset temperature of the crystal was observed at 135.6 °C with a heat of fusion of 80.8 J/g. The molten sample was then cooled at 20 °C/min to –10 °C. During this cooling process the sample does not show any exothermic

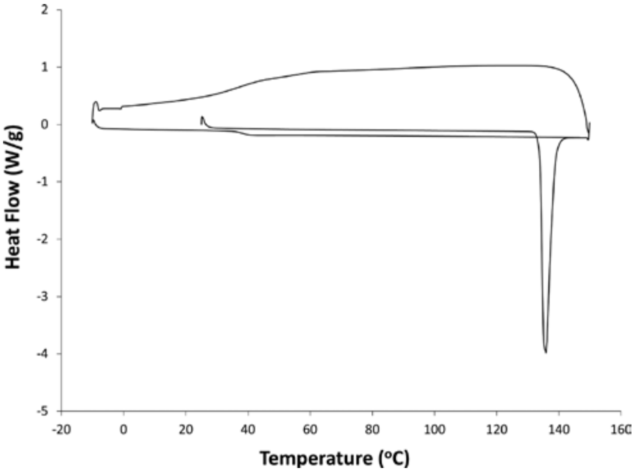

Fig. 6: DSC thermogram of 2EPNA showing the heat-cool-heat sequence.

peak, indicating the formation of an amorphous solid. On re-heating at 10 °C/min, the glass transition temperature (T_g) was observed at 38.4 °C. Furthermore, re-heating did not lead to any re-crystallization of the amorphous sample since no exothermic peak was detected. This compound exhibits good glass forming ability along with good glass stability on non-isothermal temperature treatment.

The crystalline and amorphous samples were further characterized by solid-state NMR spectroscopy. Figure 7 shows the ^{13}C SSNMR spectra of solution state, crystalline Form I, and amorphous samples of 2EPNA. Peak assignment was based on solution-phase spectra and quantum chemical calculations (Table 2). 2EPNA has two alkyl carbon atoms, C13 and C14, which are observed in the chemical

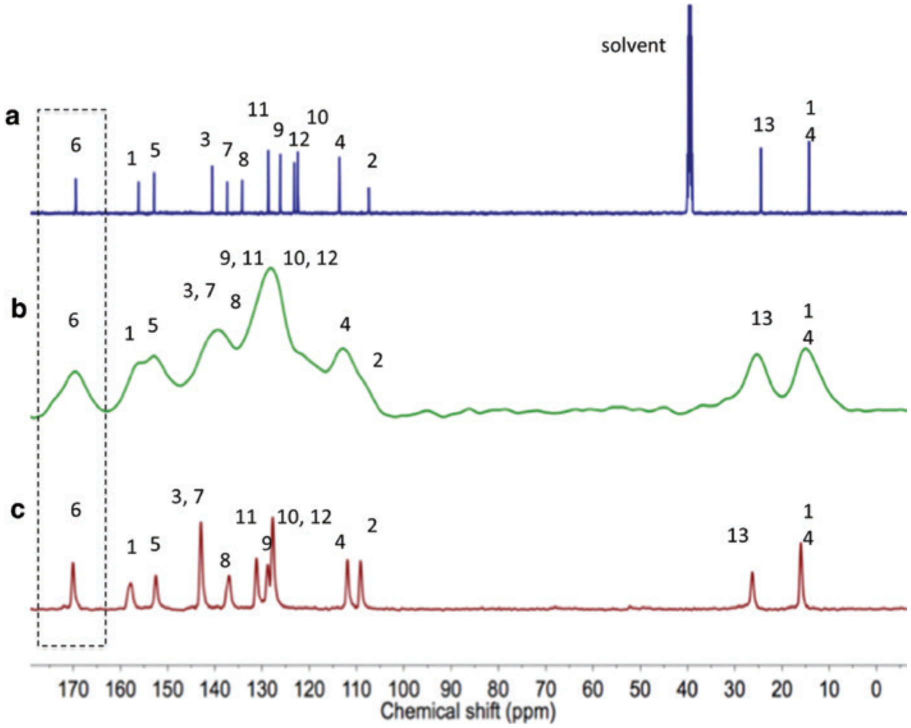

Fig. 7: ^{13}C NMR spectra of solution state (a), amorphous state (b) and crystalline state (c) of 2EPNA are presented. The solvent peak is seen at 39.9 ppm. The dashed region is of the carbonyl carbon peak which is the most characteristic of the three phases.

Tab. 2: Chemical shift assignment of 2EPNA.

Carbon number	Calculated fully optimized single molecule	Calculated monomer (H positions optimized)	Calculated dimer (H positions optimized)	δ_{sol} (ppm), solution	δ_{crys} (ppm), crystalline	δ_{amor} (ppm), amorphous
C1	162.0	163.8	161.9	156.2	157.8	155.6
C2	108.1	107.7	108.8	107.4	109.1	107.5
C3	146.9	143.8	146.5	140.6	142.9	139.5
C4	116.6	113.3	114.6	113.6	111.9	112.5
C5	160.9	160.1	160.7	152.9	152.5	152.6
C6	173.8	170.7	170.5	169.5	170.0	169.1
C7	142.7	141.9	139.6	137.4	142.9	139.5
C8	140.7	145.9	147.5	134.2	137.0	127.7
C9	135.0	132.8	134.0	126.1	128.8	127.7
C10	129.2	127.7	129.5	122.4	127.7	122.7
C11	131.0	128.3	130.4	128.7	131.1	127.7
C12	129.3	132.8	131.7	123.1	127.7	122.7
C13	30.3	31.0	32.0	24.5	26.2	25.5
C14	18.2	17.5	16.3	14.3	16.0	15.0

shift range of 10–30 ppm for the crystalline and amorphous samples. For the crystalline sample, C3 and C7 have similar resonant frequency and present broad overlapping peaks at 142.9 ppm. The remaining peaks were easily assigned based on GIAO calculations (Table 2). The amorphous sample shows broad peaks with considerable overlap seen for aromatic carbons in the region of 120–145 ppm. Sharp ^{13}C resonances generally associated with solution spectra reflect statistically averaged signals because of molecular tumbling. In the solid state, molecular motions are impeded, resulting in chemical shift peak broadening. The broader nuclear resonance distributions from the amorphous samples largely result from multiple orientations and diverse environments around carbon nuclei [36]. Because magic-angle spinning (MAS) can significantly reduce the orientation effect of dipolar coupling and chemical shielding anisotropy, it is mainly the conformational distribution of the molecules in the glassy state that leads to the NMR peak broadening [37, 38]. The carbonyl carbon (C6), which is involved in hydrogen bonding, was observed at 170.0 and 169.1 ppm for Form I and the amorphous sample respectively, indicating the similar electronic environment surrounding this carbon and the likely presence of acid-pyridine intermolecular interactions in the amorphous state. This argument is made because the crystal bears the acid-pyridine hydrogen-bonding motif.

In summary, 2EPNA provides an example of a diarylamine compound where functional group substitution on the phenyl ring provides a convenient way of controlling the polymorphic outcome. The substitution of an –ethyl group on the phenyl ring leads to formation of crystals with acid-pyridine synthons by preventing planar conformation due to steric hindrance. This relationship between synthon and conformation has been observed for other compounds examined in previous studies [13–16]. Furthermore, the hydrogen-bonding motif was also present in the amorphous state, which likely impedes the recrystallization from the amorphous state. Alignment of these hydrogen bonding chains into a three-dimensional lattice (i.e. a crystal) appears to present a kinetic barrier for crystallization.

Acknowledgments: The authors thank Chao Endowment and Purdue Research Foundation (PRF) for supporting this project.

References

[1] K. Naito, P. Miura, Molecular design for nonpolymieric organic dye glasses with thermal stability: relations between thermodynamic parameters and amorphous properties. *J. Phys. Chem.* **1993**, *97*, 6240.

[2] R. Wang, C. Pellerin, O. Lebel, Role of hydrogen bonding in the formation of glasses by small molecules: a triazine case study. *J. Mater. Chem.* **2009**, *19*, 2747.

[3] J. D. Wuest, O. Lebel, Anarchy in the solid state: structural dependence on glass-forming ability in triazine-based molecular glasses. *Tetrahedron* **2009**, *65*, 7393.

[4] J. A. Baird, B. Van Eerdenbrugh, L. S. Taylor, A classification system to assess the crystallization tendency of organic molecules from undercooled melts. *J. Pharm. Sci.* **2010**, *99*, 3787.

[5] A. R. Oganov, A. O. Lyakhov, M. Valle, How evolutionary crystal structure prediction works-and why. *Acc. Chem. Res.* **2011**, *44*, 227.

[6] S. L. Price, Computed crystal energy landscapes for understanding and predicting organic crystal structures and polymorphism. *Acc. Chem. Res.* **2009**, *42*, 117.

[7] S. M. Woodley, R. Catlow, Crystal structure prediction from first principles. *Nat. Mater.* **2008**, *7*, 937.

[8] R. W. Hartel, *Crystallization in Foods*. 1st ed. Food Engineering Series. Springer, USA, **2001**.

[9] N. J. Babu, A. Nangia, Solubility advantage of amorphous drugs and pharmaceutical cocrystals. *Cryst. Growth Des.* **2011**, *11*, 2662.

[10] S. Bates, G. Zografi, D. Engers, K. Morris, K. Crowley, A. Newman, Analysis of amorphous and nanocrystalline solids from their X-ray diffraction patterns. *Pharm. Res.* **2006**, *23*, 2333.

[11] T. Matsumoto, G. Zografi, Physical properties of solid molecular dispersions of indomethacin with poly(vinylpyrrolidone) and poly(vinylpyrrolidone-co-vinyl-acetate) in relation to indomethacin crystallization. *Pharm. Res.* **1999**, *16*, 1722.

[12] A. Newman, G. Knipp, G. Zografi, Assessing the performance of amorphous solid dispersions. *J. Pharm. Sci.* **2012**, *101*, 1355.

[13] S. H. Long, S. Parkin, M. A. Siegler, A. Cammers, T. L. Li, Polymorphism and phase behaviors of 2-(phenylamino)nicotinic acid. *Cryst. Growth Des.* **2008**, *8*, 4006.

[14] S. H. Long, S. Parkin, M. Siegler, C. P. Brock, A. Cammers, T. L. Li, Polymorphism of an organic system effected by the directionality of hydrogen-bonding chains. *Cryst. Growth Des.* **2008**, *8*, 3137.

[15] S. H. Long, T. L. Li, Controlled formation of the acid-pyridine heterosynthon over the acid-acid homosynthon in 2-anilinonicotinic acids. *Cryst. Growth Des.* **2009**, *9*, 4993.

[16] S. H. Long, T. Li, Enforcing molecule's pi-conjugation and consequent formation of the acid-acid homosynthon over the acid-pyridine heterosynthon in 2-anilinonicotinic acids. *Cryst. Growth Des.* **2010**, *10*, 2465.

[17] A. Kalra, P. Tishmack, J. W. Lubach, E. Munson, L. S. Taylor, S. R. Byrn, T. Li, Impact of supramolecular aggregation on the crystallization kinetics of organic compounds from the supercooled liquid state. *Mol. Pharmacol.* **2017**, *14*, 2126.

[18] Bruker, *"APEX2" Bruker-AXS*, Madison, WI, USA, **2006**.

[19] L. Krause, R. Herbst-Irmer, G. M. Sheldrick, D. Stalke, Comparison of silver and molybdenum microfocus X-ray sources for single-crystal structure determination. *J. Appl. Crystallogr.* **2015**, *48*, 3.

[20] G. M. Sheldrick, SHELXT – Integrated space-group and crystal-structure determination. *Acta Crystallogr. A* **2015**, *71*, 3.

[21] G. M. Sheldrick, Crystal structure refinement with SHELXL. *Acta Crystallogr. C* **2015**, *71*, 3.

[22] S. Parkin, Expansion of scalar validation criteria to three dimensions: the R tensor. *Acta Crystallogr. A* **2000**, *56*, 157.

[23] A. L. Spek, Structure validation in chemical crystallography. *Acta Crystallogr. D* **2009**, *65*, 148.

[24] A. J. C. Wilson, *International Tables for Crystallography*, *Vol C: Mathematical, Physical and Chemical Tables*. Kluwer Academic Publishers, Holland, **1992**.

[25] R. Ditchfie, Self-consistent perturbation-theory of diamagnetism. 1. Gauge-invariant lcao method for nmr chemical-shifts. *Mol. Phys.* **1974**, *27*, 789.

[26] K. Wolinski, J. F. Hinton, P. Pulay, Efficient implementation of the gauge-independent atomic orbital method for nmr chemical-shift calculations. *J. Am. Chem. Soc.* **1990**, *112*, 8251.

[27] J. R. Cheeseman, G. W. Trucks, T. A. Keith, M. J. Frisch, A comparison of models for calculating nuclear magnetic resonance shielding tensors. *J. Chem. Phys.* **1996**, *104*, 5497.

[28] L. B. Casabianca, A. C. De Dios, Ab initio calculations of NMR chemical shifts. *J. Chem. Phys.* **2008**, *128*, 10.

[29] J. C. Facelli, Calculations of chemical shieldings: theory and applcations. *Concepts in Magnetic Resonance Part A* **2004**, *20A*, 42.

[30] M. J. Frisch, G. W. Trucks, H. B. Schlegel, G. E. Scuseria, M. A. Robb, J. R. Cheeseman, G. Scalmani, V. Barone, B. Mennucci, G. A. Petersson, H. Nakatsuji, M. Caricato, X. Li, H. P. Hratchian, A. F. Izmaylov, J. Bloino, G. Zheng, J. L. Sonnenberg, M. Hada, M. Ehara, K. Toyota, R. Fukuda, J. Hasegawa, M. Ishida, T. Nakajima, Y. Honda, O. Kitao, H. Nakai, T. Vreven, J. A. Montgomery, Jr., J. E. Peralta, F. Ogliaro, M. Bearpark, J. J. Heyd, E. Brothers, K. N. Kudin, V. N. Staroverov, R. Kobayashi, J. Normand, K. Raghavachari, A. Rendell, J. C. Burant, S. S. Iyengar, J. Tomasi, M. Cossi, N. Rega, N. J. Millam, M. Klene, J. E. Knox, J. B. Cross, V. Bakken, C. Adamo, J. Jaramillo, R. Gomperts, R. E. Stratmann, O. Yazyev, A. J. Austin, R. Cammi, C. Pomelli, J. W. Ochterski, R. L. Martin, K. Morokuma, V. G. Zakrzewski, G. A. Voth, P. Salvador, J. J. Dannenberg, S. Dapprich, A. D. Daniels, Ö. Farkas, J. B. Foresman, J. V. Ortiz, J. Cioslowski, D. J. Fox, *Gaussian 09, Revision C.01*. Gaussian, Inc., Wallingford, CT, **2009**.

[31] R. Dovesi, R. Orlando, B. Civalleri, C. Roetti, V. R. Saunders, C. M. Zicovich-Wilson, *Z. Kristallogr.* **2005**, *220*, 571.

[32] D. Thompson, J. Braun, R. Ford, *OpenDX: Paths to Visuallization*, VIS, Inc., Missoula, MT, **2001**.

[33] M. C. Etter, Encoding and decoding hydrogen-bond patterns of organic compounds. *Acc. Chem. Res.* **1990**, *23*, 120.

[34] M. Zhang, T. Li, Intermolecular interactions in organic crystals: gaining insight from electronic structure analysis by density functional theory. *CrystEngComm* **2014**, *16*, 7162.

[35] C. Morell, A. Grand, A. Toro-Labbe, New dual descriptor for chemical reactivity. *J. Phys. Chem. A* **2005**, *109*, 205.

[36] R. H. Tromp, D. Van Dusschoten, R. Parker, S. G. Ring, Carbon-13 nuclear magnetic relaxation in supercooled liquid and glassy maltose. *Phys. Chem. Chem. Phys.* **1999**, *1*, 1927.

[37] R. Lefort, P. Bordat, A. Cesaro, M. Descamps, Exploring conformational energy landscape of glassy disaccharides by cross polarization magic angle spinning C-13 NMR and numerical simulations. I. Methodological aspects. *J. Chem. Phys.* **2007**, *126*, 9.

[38] J. Baronsky, M. Preu, M. Traeubel, N. A. Urbanetz, Perfusion calorimetry in the characterization of solvates forming isomorphic desolvates. *Eur. J. Pharm. Sci.* **2011**, *44*, 74.

Supplemental Material: The online version of this article offers supplementary material (https://doi.org/10.1515/zkri-2017-2070).